Appl. Phys. A (2015) 121:343–356
DOI 10.1007/s00339-015-9229-6

Applied Physics A
Materials Science & Processing

CrossMark

INVITED PAPER

A step toward next-generation nanoimprint lithography: extending productivity and applicability

Jong G. Ok[1] · Young Jae Shin[2] · Hui Joon Park[3] · L. Jay Guo[4]

Received: 14 March 2015 / Accepted: 8 May 2015 / Published online: 27 May 2015
© Springer-Verlag Berlin Heidelberg 2015

Abstract Because of its unique principle based on mechanical deformation, nanoimprint lithography (NIL) has been playing an important role for nanopatterning and nanofabrication beyond the limit of conventional optical lithography. Many diverse fields involving electronics, photonics, and energy engineering have all shown significant increase in utilization of nanopattern structures, particularly in large areas and at submicron scales. To meet this demand, expanding the realm of NIL toward more scalable and versatile patterning technology is in high demand. In this feature article, we give an overview of how NIL can extend productivity and applicability by addressing three key issues: continuous NIL for more scalable nanopatterning, large-area mold fabrications, and novel resist engineering.

✉ Jong G. Ok
jgok@seoultech.ac.kr

✉ Hui Joon Park
huijoon@ajou.ac.kr

✉ L. Jay Guo
guo@umich.edu

[1] Department of Mechanical and Automotive Engineering, Seoul National University of Science and Technology, Seoul 139-743, Korea

[2] Department of Electrical and Systems Engineering, University of Pennsylvania, Philadelphia, PA 19104, USA

[3] Division of Energy Systems Research, Ajou University, Suwon 443-749, Korea

[4] Department of Mechanical Engineering; Electrical Engineering and Computer Science, University of Michigan, Ann Arbor, MI 48109, USA

1 Introduction

In many fields, nanoimprint lithography (NIL) has served to create and replicate nanoscale patterns and structures beyond the limit of typical optical and e-beam lithography [1, 2]. Free from optical diffraction and beam scattering that limits the patterning resolution, NIL makes use of various schemes of direct mechanical deformation of a target substrate by using a proper mold (stamp). For instance, heat and pressure are applied between a mold and a thermoplastic to thermally imprint desired pattern (i.e., thermal NIL) [3, 4], or UV light is illuminated on the UV-curable resist coated on a desired substrate under a mold contact to solidify the mold-engaged resist structure (i.e., UV NIL) [5, 6]. Many variations based on these two main NIL concepts have been presented for reliable and high-resolution nanopatterning. While all these techniques are effective for certain uses (e.g., small-footprint devices and chips), there still remain several challenges on NIL as nanopatterns are being utilized in applications, particularly requiring larger areas and smaller periods [6–8]. To this end, we review three areas of research toward more productive and wide-applicable nanopatterning methodology: (1) continuous roll-to-roll nanoimprinting process, (2) methods for preparing large-area molds, and (3) novel resist materials engineering for smaller patterns with higher mechanical integrity.

2 Continuous and scalable roll-to-roll nanoimprinting

Expanding the fabrication throughput of the conventional NIL, more scalable nanopatterning processes based on continuous processing principles can be devised.

Implementing the continuous processing in small scale may not necessarily lean on complex and expensive nanofabrication, but can be inspired by the traditions of continuous mechanical machining processes such as rolling, pullout, and forging [8]. This section will describe how the nanopatterning can increase fabrication throughput and extend the range of applicable features.

Roll-to-Roll (R2R) NIL adopts the principle of rolling process to continuous nanopatterning [9–11]. Figure 1a shows the schematics of the R2R NIL process [10]. A flexible mold with the desired surface relief pattern is wrapped around a roll. Here, the large-area mold can be scaled up by tiling small master stamps until it can wrap the roll. Another roll conveys a substrate, which is usually coated with a UV-curable resist before entering the mold contact zone (i.e., nip). These two rolling cylinders ensure a conformal contact between the mold and the resist surface, continuously printing the desired pattern into the resist on the substrate. The UV light at the outlet of nip instantly cures the resist to complete the patterning. In case the rigid substrate is desired, the R2R mode can be readily converted to roll-to-plate (R2P) configuration where the substrate-carrying roll is replaced by the plate conveyor. The nature of continuous process allows UV NIL that can instantly define the pattern to best suit for R2R NIL rather than thermal NIL.

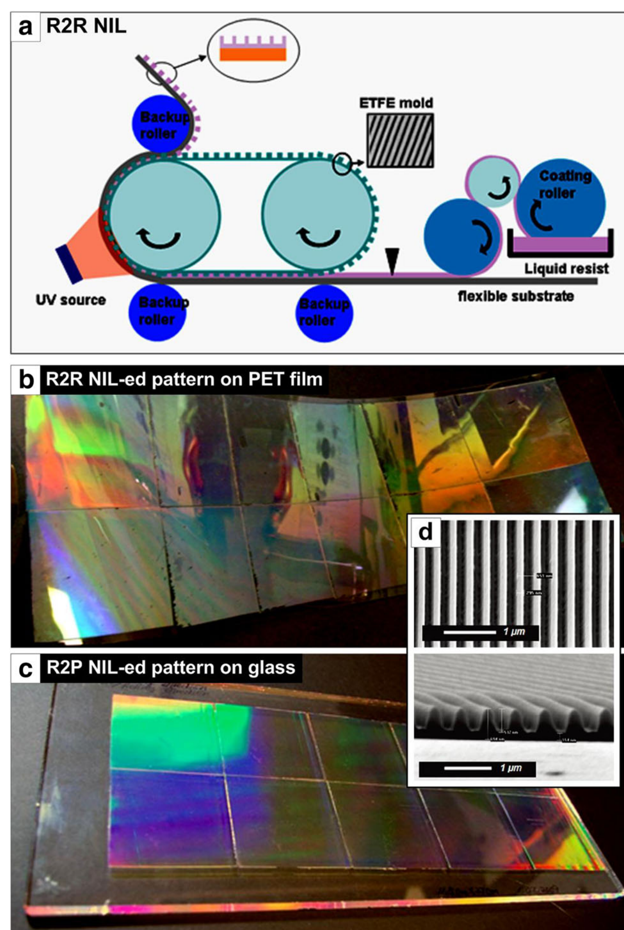

Fig. 1 **a** Schematic illustration of R2R NIL process. Large-area grating patterns fabricated on **b** flexible polyethylene terephthalate (PET) and **c** rigid glass substrates. **d** Scanning electron microscope (SEM) images of the imprinted pattern (reproduced from Ref. [10] with permission from the American Chemical Society)

R2R/R2P NIL can continuously churn out large-area nanopatterns of various shapes either on a flexible (Fig. 1b) or on a rigid (Fig. 1c) substrate. As will be discussed in detail later, many applications requiring large areas, flexibility, and high throughput, including flexible photovoltaic cells [12], optical polarizer films [13], and metamaterial coatings [11], can benefit from R2R NIL. On the other hand, the following requirements need to be satisfied to enable R2R NIL: First, the mold large enough to cover the roll should be prepared; second, the seam generated where the two ends of a wrapped mold meets should be overcome; third, the resist should be well prepared so as to cure promptly and to have strong adhesion to the substrate but low adhesion to the mold. These requirements could be addressed, e.g., by making large-area seamless molds, introducing the alternative seamless patterning processes, or carefully engineering the resists, which will be addressed in the following sections.

3 Methods for preparing large-area molds

Apart from typical methods of making the original molds by photolithography, electron-beam lithography, or interference lithography, we would like to suggest a few alternative patterning processes that can produce large-area nanostructures, especially suitable for R2R process.

3.1 Seamless and scalable nanopatterning methodologies

Analogous to traditional pullout process, dynamic nanoinscribing (DNI) [14] and nanochannel-guided lithography (NCL) [15] deform and squeeze the substrate material in the shape of grating pattern through the openings in the grating mold (Fig. 2a). The cleaved mold edge is mounted in a proper angle over the substrate and then is lowered down to make a conformal contact with the substrate under adequate pressure and temperature. Here, the shape of the tool edge is usually designed to be the high-aspect-ratio rectangular grating so that the grating valleys do not touch the substrate while the grating hills press the substrate. As the tool moves linearly (or along the arbitrary route) while maintaining the conformal contact with the substrate, the substrate surface is patterned to the grating

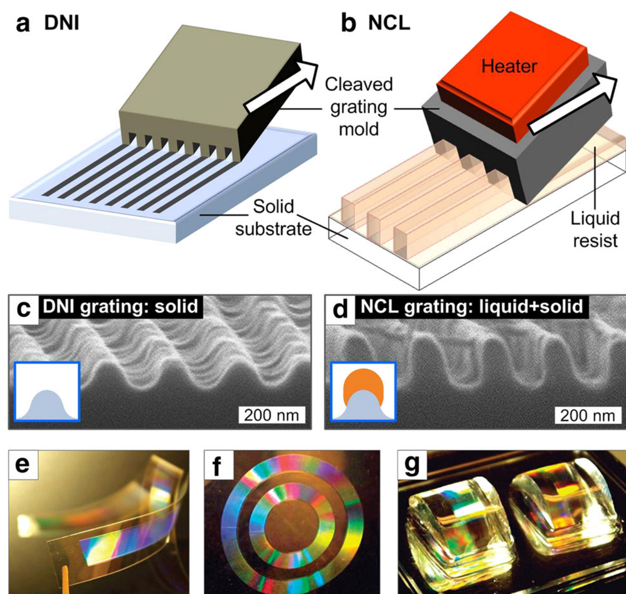

Fig. 2 Schematic descriptions of **a** DNI and **b** NCL processes. SEM images of the resulting grating patterns processed under the identical conditions [temperature = 80 °C, substrate material = perfluoroalkoxy (PFA)] reveal that the **d** NCL-processed grating can have higher aspect ratio compared with the **c** DNI-processed one. DNI can perform seamless nanopatterning on **e** long PET web, create **f** nonlinear pattern, and make patterns on **g** *curved surface* (**b**–**d** reproduced from Ref. [15] with permission from John Wiley and Sons; (**e**, **f**): reproduced from Ref. [14] with permission from the American Chemical Society)

structure. DNI employs a solid polymer substrate only, while in NCL the viscous UV-curable liquid coating is applied on the substrate (Fig. 2b). DNI and NCL realize continuous nanograting fabrication without seams. While both DNI and NCL mainly base on the plastic deformation of the substrate for which the compliant polymer thus best suits, NCL can achieve higher-aspect-ratio patterns by adding liquid blocks on top of the solid groove structures (Fig. 2c, d). Though the prefabrication of grating molds is still necessary, the fabrication throughput and applicability can be significantly enhanced as what we need is just an edge, not a spacious stamp.

As another scalable nanopatterning method, vibrational indentation patterning (VIP) [16] achieves mold-free, period-tunable nanopatterning by utilizing high-frequency vibration of a flat tool edge (Fig. 3a), eliminating the need of prefabricated molds. Like traditional forging/indentation, the vertically vibrating tool edge (typically silicon nitride or engineering diamond) periodically indents the lines on the linearly moving substrate. VIP can practically provide a wide range of special nanopatterning solutions. The substrate can be any materials softer than a tool, allowing the direct patterning onto a metal-coated polymer (Fig. 3b) or a polyimide film that otherwise is difficult to pattern (Fig. 3c). Most remarkably, the resulting grating

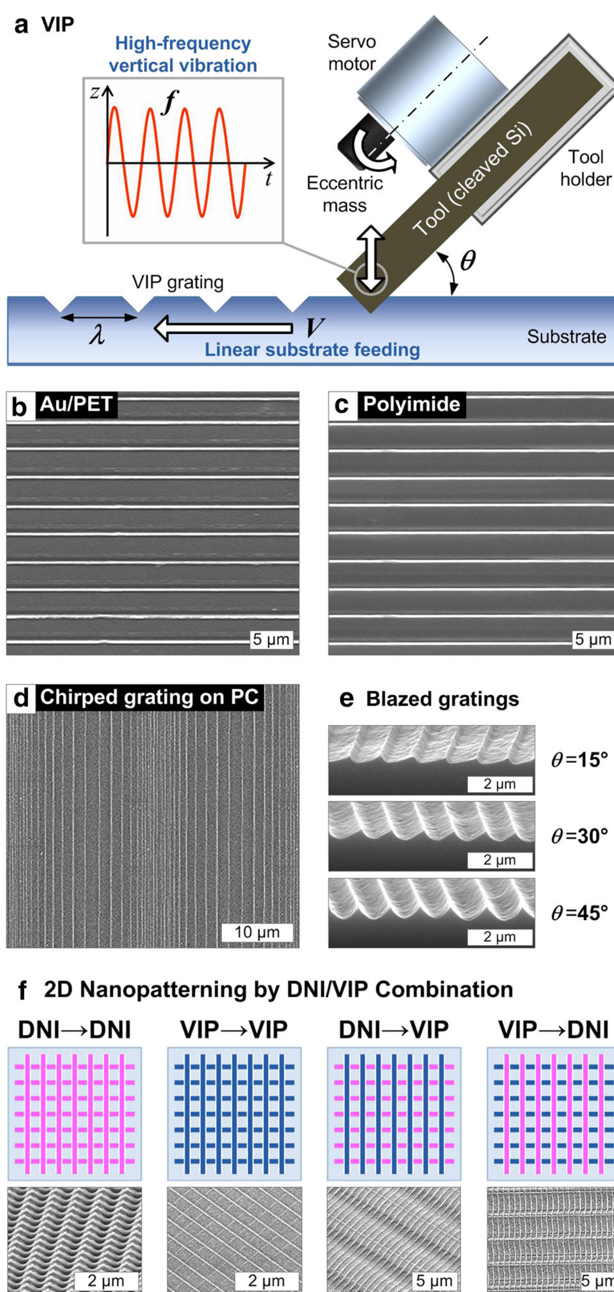

Fig. 3 **a** Schematic drawing of VIP process. Various patterns created by VIP: grating patterns on **b** Au/PET and **c** polyimide (Kapton) films, **d** chirped grating formed on polycarbonate (PC), and **e** blazed gratings with various blazed angles made on PC films. **f** Continuous fabrication of two-dimensional (2D) patterns through sequential 1D patterning strokes enabled by DNI and VIP (**a**–**e** reproduced from Ref. [16] with permission from John Wiley and Sons; **f** reproduced from Ref. [17] with permission from the Royal Society of Chemistry)

pattern period can be tuned in real-time basis (i.e., chirped grating; Fig. 3d) simply by controlling the tool vibration frequency and substrate feeding speed. VIP generates ‘saw-tooth’-like blazed gratings; the blazed angle can also be regulated simply by adjusting the mounting angle of the tool (Fig. 3e). Since VIP uses a flat edge, its manufacturing

throughput is dramatically improved. Also attributed to its simple but versatile operation principle, the period, blazed angle, and dimension can be readily controlled.

3.2 Use of DNI/NCL and VIP for R2R mold fabrication: potentials and challenges

As DNI and NCL are essentially based on 2D contact, not only can the linear grating be made (Fig. 2e), but the nonlinear grating pattern can also be created on curved surfaces (Fig. 2f, g) [8]. VIP can also produce various patterns over large areas without resorting to preparation of multiple tools or masters. Further, by performing two VIP processes (and/or DNI processes) sequentially in the orthogonal direction, 2D mesh patterns can be easily created (Fig. 3f) [17]. Hence, DNI/NCL and VIP can be potentially adopted to prepare the large-area R2R NIL molds. For instance, DNI/NCL can be directly performed over the curved roll surface, or DNI/VIP can be used to create scalable master films containing diverse multidimensional patterns that can be wrapped around the roll.

Although DNI/NCL and VIP enable continuous and seamless fabrication of nanograting patterns, more diverse nanopatterns other than gratings, such as dots and holes, are requested in many applications. In particular, interests in tens of nanometer-scale dot/hole patterns have continuously increased due to their potential applications for novel materials and devices [18–20]. It has been shown that NIL-based processes can be utilized to produce tens of nanometer-scale structures in large-area format within short processing time. However, one of the prerequisites is the preparation of NIL molds having the comparable dimensions to the targeted structures. Therefore, making large-area molds containing not only gratings but also more various patterns, targeting R2R NIL and other scalable nanopatterning processes, is called for. This section presents several methods to prepare large-area molds without relying on time-taking e-beam lithography or laser interferometry.

3.3 Visually tolerable tiling for large-area R2R molds

As aforementioned, the seam appearance in molds is one of the biggest issues to resolve in R2R NIL, especially the imprinted structures are aimed for optical (e.g., display) applications, as any seam lines whose widths are greater than a few microns can be detected by human eyes. While the seam cannot be completely removed, one realistic strategy is to make it invisible to the naked eyes so that the imprinted replica can be practically applied to many optical films and display applications.

Such a strategy is materialized in the novel tiling technique named visually tolerable tiling (VTT; Fig. 4) [21] where the stitching seams generating between each small master stamp tile are successfully suppressed within 500-nm regime that is unperceivable to human eyes. In VTT, the small master pattern tiles are stamped in a slightly overlapped manner (Fig. 4b) using a properly designed UV-curable resist; the uncured resist should not spread but dewet on the cured resist surface to minimize seams; and polyurethaneacrylate (PUA) possesses such a characteristic [22] and is used for this demonstration. Figure 4a depicts the overall VTT procedure; once the first tile is stamped and cured using the resist, the uncured resist is dropped nearby. Then, the second tiling is performed under pressure such that the mechanically squeezed thin layer of uncured resist slightly overflows over the boundary of the cured (and patterned) surface, followed by curing. The dewetting characteristics of uncured resist keep the new boundary of the second tile less than 500 nm (Fig. 4c, d). By properly conditioning the resin (e.g., viscosity, drop amount) and stamping (e.g., pressure), the vertical height of each boundary can also be controlled within than 500 nm [21].

The VTT-fabricated large-area stamps and replicas can serve as flexible R2R molds or other large-area nanopatterning masters. Further, VTT can potentially resolve the seam issue in R2R NIL; VTT using a flexible tile stamp can be performed around the roll surface until the patterned tiles entirely wrap the roll. Such techniques can pursue practical fabrication of scalable optical device components such as polarizers for large-area televisions.

3.4 Tens of nanometer-scale large-area mold fabrication using self-assembly of block copolymers

To fabricate tens of nanometer-scale nanostructures, which conventional photolithography has a limitation to access, electron-beam lithography and focused ion beam (FIB) lithography have been widely utilized. However, the long processing time and the high cost limit the further application of those methods to large-area nanopatterns. Alternatively, nanotemplates such as anodized aluminum oxide (AAO) and track-etched membrane have been utilized to prepare nanopatterns, but the difficulty in removing the templates and the weak adhesion between template and substrate remains the issues to be resolved [23, 24].

During last few decades, the self-assembly property of block copolymer have been highlighted as a promising candidate to access tens of nanometer-scale nanostructures [25, 26]. Because different polymer blocks, having repulsion between incompatible polymer blocks, are connected by covalent bonds, inducing internal segregation, periodic nanostructures can be spontaneously generated by nanoscale phase separation. Furthermore, various technologies that can control the orientation of those nanostructures

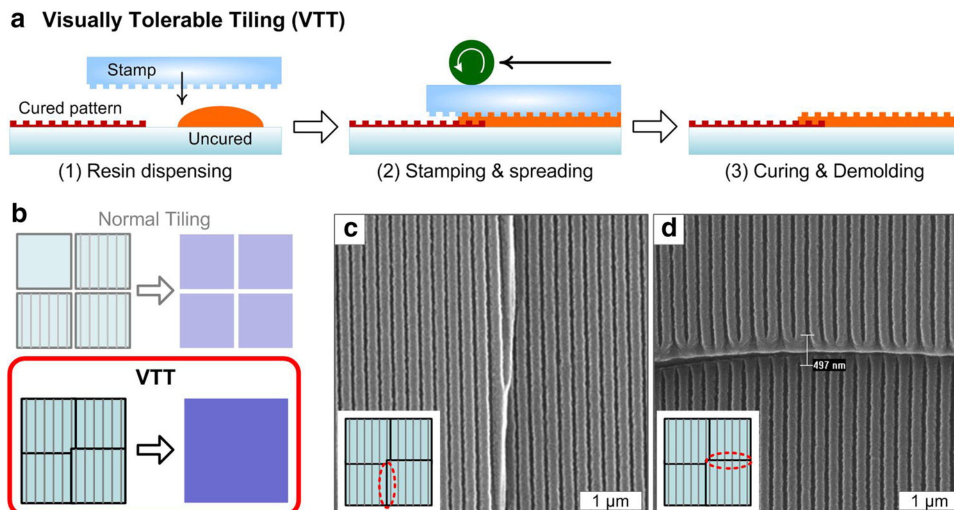

Fig. 4 **a** Schematics of the VTT procedure. **b** Comparative illustrations of normal tiling (*top* and *shaded*) and VTT (*bottom*). SEM images of **c** *vertical* and **d** *horizontal* seams between two tiles stitched using VTT (reproduced from Ref. [21] with permission from the Royal Society of Chemistry)

make it possible for this polymer system to be used for thin film nanotemplate fabrication [25, 27, 28]. Since it is based on physical and chemical interaction of the polymer blocks within the material rather than requiring external patterning, in principle the process can be scaled up to large areas [29, 30]. Figure 5a illustrates the exemplary process to prepare sub-20-nm-scale NIL molds using the self-assembled nanostructures of diblock copolymer [20]. In this system, poly(styrene)-*block*-poly(methyl methacrylate) (PS-*b*-PMMA) diblock copolymer with 0.7 volume fraction of PS that can give equilibrated morphology of hexagonally packed cylinders having about 20 nm domain size was utilized, and several nanometers thick poly(-styrene-*ran*-methyl methacrylate) (PS-*r*-PMMA) random copolymer was cast on the substrate to produce the neutral surface to PS and PMMA, consequently leading to vertically oriented cylindrical PMMA nanodomains surrounded by PS [Fig. 5a:(a)]. Subsequent O_2 plasma etching gave porous PS nanotemplate due to the etching selectivity between PS and PMMA, about 1:1.5 $\sim$ 2 to O_2 plasma etching [Fig. 5a:(b)], and those resultant nanotemplates could be used to fabricate nanohole- and nanopillar-type SiO_2 NIL molds. To prepare nanohole-type SiO_2 nanostructures, a Cr mask, highly resistant to the reactive ion etching (RIE) gases used to etch oxide, was selectively added on the top surface of PS template using angled deposition to reinforce the PS template to RIE, and following RIE could give almost 1:10 aspect ratio SiO_2 nanoholes [Fig. 5a:(1c–e)], b). As for nanopillar-type SiO_2 nanostructure, Cr was normally deposited on PS nanotemplate to insert Cr inside the template, and the additional mild Cr RIE etching step facilitated following liftoff process by eliminating excess Cr on the top surface as well as the sidewall of PS template. Consequently, remaining Cr nanodots on the surface of SiO_2 layer after liftoff process were utilized as etch mask to prepare SiO_2 nanopillar structures [Fig. 5a:(2c–f)], and the resultant SiO_2 nanopillar structures with about 1:10 aspect ratio are shown in Fig. 5c. These nanostructures could be successfully utilized as NIL molds, and imprinted structures, prepared by thermal NIL process using these molds of both hole and pillar polarities, are represented in Fig. 5d [poly(3-hexylthiophene-2,5-diyl) (P3HT)] and Fig. 5e (PMMA), respectively.

4 Resist engineering for more functional and smaller-scale patterning

Making the nanopatterns denser and smaller, preferably with higher aspect ratios, is crucial to provide key functions in many emerging technologies, for instance to utilize the large surface-to-volume ratios [31]. Also, strategies to create nanoscale patterns of functional inorganics are highly desired for broader applications. Realizing these concepts may be directly connected to the engineering of novel NIL resists and processing chemistry, which will be discussed in this section with three key components: post-NIL resist shrinking, flexible resist for ultra-high-aspect-ratio nanostructure, and functional inorganic–organic hybrid resist.

4.1 Shrinkable resists for slenderized NIL

Epoxysilsesquioxane (SSQ)-based materials had been synthesized for large-area and high-resolution NIL. SSQ possesses many appropriate properties as the NIL resist, such as great coatability, high modulus, good mold release, and excellent dry etch resistance. Because of epoxy functional groups, the UV-curable SSQ can be developed by mixing adequate amount of photoinitiators to make curing time very short at room temperature [32].

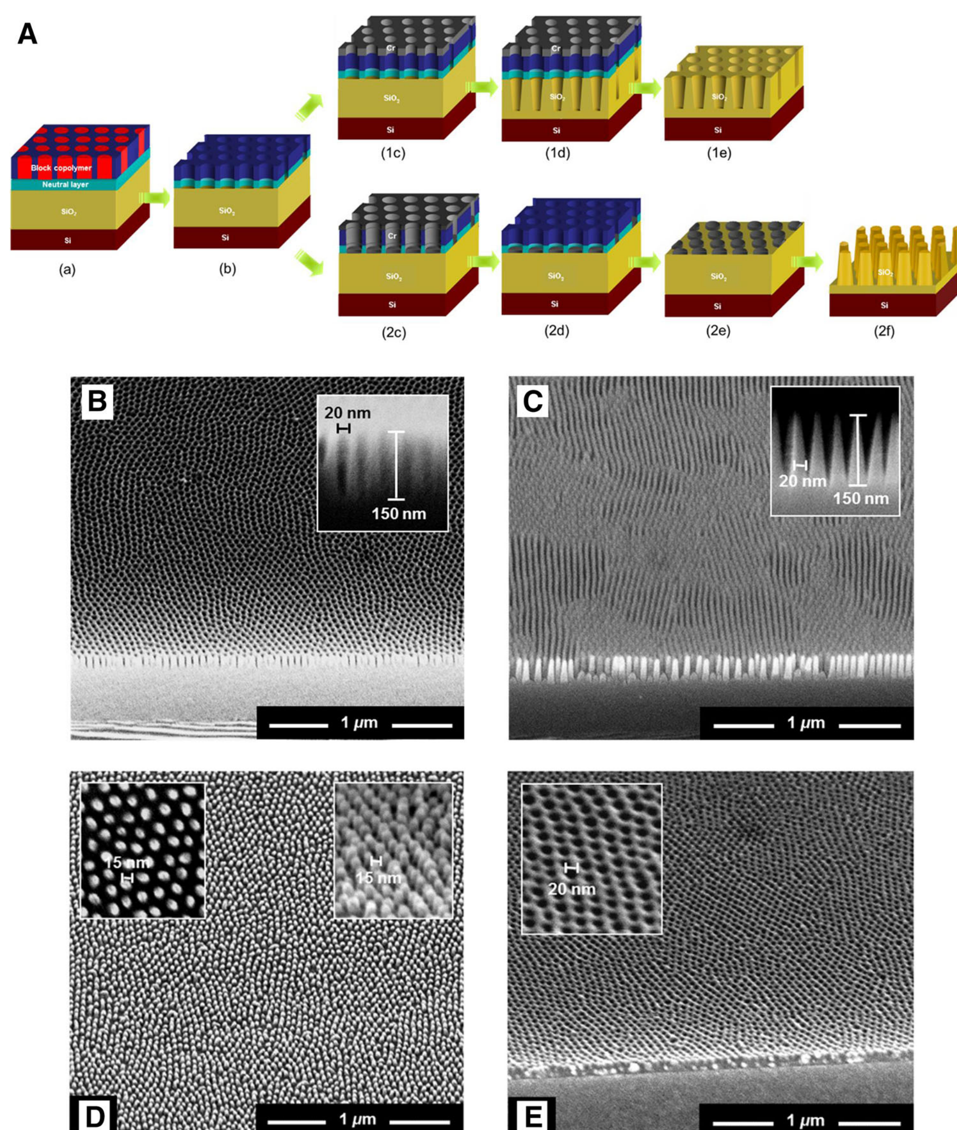

Fig. 5 **A**. Schematic of the process for fabricating both nanohole and nanopillar array patterns in SiO_2: **a** cylindrical PS-*b*-PMMA morphology is developed on the substrate surface modified by the neutral PS-*r*-PMMA layer. **b** PMMA nanodomains are selectively removed by O_2 plasma etching. Nanohole array fabrication process; 1**c** Cr is selectively deposited on polymer template using shadow evaporation; 1**d** SiO_2 layer is etched using Cr mask by RIE; 1**e** Cr mask and polymer template are removed for SiO_2 and form nanohole arrays. Nanopillar array fabrication process; 2**c** Cr is deposited over the polymer template; 2**d** top Cr layer is removed by Cr etching RIE; 2**e** Cr nanodots remained after liftoff; 2**f** SiO_2 layer is etched using Cr mask by RIE, and Cr masks are subsequently removed. **B**. SiO_2 nanohole structure. **C**. SiO_2 nanopillar structure. **D**. SEM micrographs of imprinted poly(3-hexylthiophene-2,5-diyl) (P3HT) nanopillars with 15 nm diameter (aspect ratio $\sim$2.5) taken at 45° tilted view. The inset images on the left and right provide high-magnification top view and 75° tilted view, respectively. **E**. SEM micrographs of PMMA nanotemplate imprinted by SiO_2 nanopillar mold. Inset images are the high-magnification SEM images, and images are 45° tilted views (reproduced from Ref. [20] with permission from the American Chemical Society)

The SSQ-based resist, once imprinted, can be shrunk by a simple heating process, thereby tailoring the pattern geometry to smaller scales. Figure 6 shows the thermally treated SSQ patterns whose widths are reduced upon heat treatment. Many diverse pattern shapes such as gratings (Fig. 6a–c) and dots (Fig. 6d, e) can be shrunk to smaller structures. This is attributed to the thermal decomposition of the organic groups in inorganic–organic hybrid SSQ at high temperature and condensation reactions [33], as can be verified in thermogravimetric analysis (TGA; Fig. 6f) and by IR spectroscopy. The condensation reaction between residual silanol groups from the SSQ resins and releasing water helps nanostructures shrinking as well [34]. The film thickness is also reduced during the thermal shrinking process (Fig. 6g) [33], which can aid the device flexibility as the SSQ thin film is free from cracking with the thickness <1 μm.

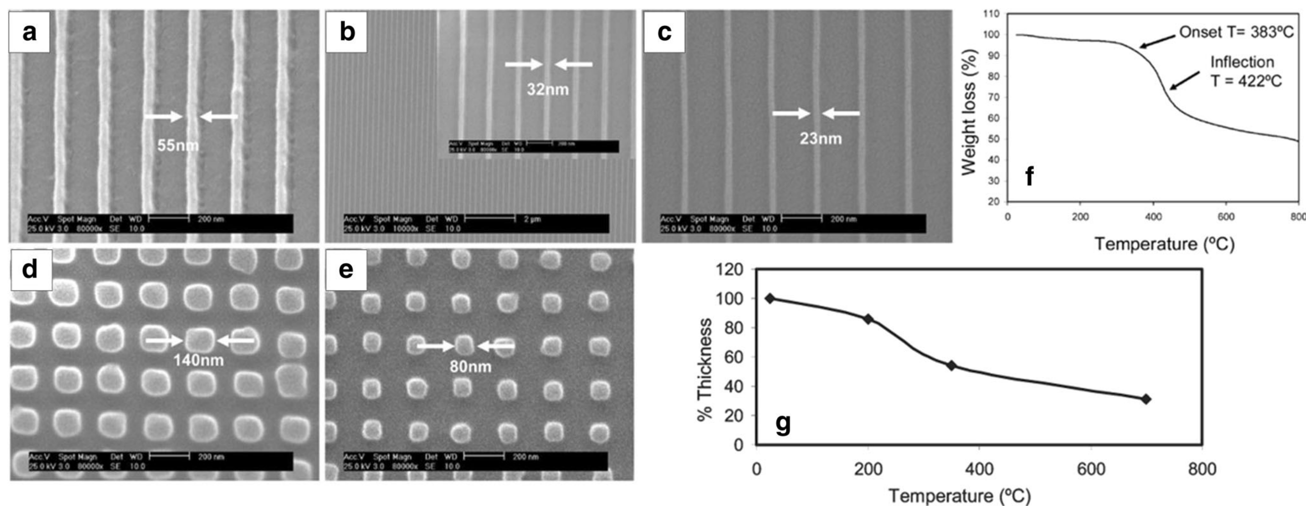

Fig. 6 **a** Control grating sample of 220 nm period and 55 nm *line* width, **b** the grating sample heated to 350 °C (*line* width is 32 nm), **c** the grating sample heated to 700 °C (*line* width is 23 nm), **d** control nanopillars sample of 140 nm size, **e** the nanopillar sample heated to 700 °C (pilar size is 80 nm), **f** TGA of the epoxy-SSQ (SSQ-A), **g** film thickness plot measured by ellipsometry for reference and heat-treated samples (reproduced from Ref. [33] with permission from the American Chemical Society)

4.2 Flexible resists for ultra-high-aspect-ratio NIL

Imprinting using hard molds such as Si can achieve sub-20-nm resolution in normal NIL [35], but requires very flat and clean surface condition as well as high pressure to ensure high yield and good quality of nanopatterns [36]. The soft lithography, adopting flexible molds made of such as PDMS, does not necessarily require high pressure or ideally flat surfaces, making the NIL process more affordable. In order to make the nanostructures having small period and high aspect ratio by NIL using soft molds, appropriate properties of NIL resist is necessary. For example, if its modulus is too high in the cured state, it is good for fabricating tens of nanometer-scale nanostructures, yet is too brittle to achieve high aspect ratios. If it is too soft, the resolution limitation of nanostructures becomes a roadblock like found in PDMS [37].

To address this issue, and in case that a single material cannot easily meet flexibility and modulus at the same time, a proper formulation of multiple resist materials mixture can be developed [38], targeting ultra-small-scale NIL patterning. Figure 7 shows one example of the NIL fabrication of high-aspect-ratio, sub-20-nm-width nanograting patterns (Fig. 7a, b) using the mixture of bisphenol F-type epoxy resin and NBR-based epoxy resin [39]. The curing time is typically less than a minute, which can be further reduced to a few seconds by regulating the concentration of photoacid generator. In cured state, bisphenol F-type resin increases modulus due to benzene rings inside of molecules; in contrast, NBR resin increases rubbery properties (Fig. 7c). The optimal ratio of mixture of these two materials renders the imprinted structure flexible enough to realize high aspect ratios and rigid enough to support small-scale features without buckling.

4.3 NIL of functional inorganic–organic hybrid resists

Besides polymeric materials that typically best suits for NIL, inorganic materials patterns will broaden the applicability of NIL. Imprinting of inorganic materials, however, will be tricky because they are usually too hard and brittle to bear direct mechanical deformation. One promising way to make patterns of inorganic materials by NIL will be to make the hybrid resist by mixing inorganic material powders with malleable organic resin and remove the organic material after NIL, e.g., by heat treatment. One exemplary work regarding titanium oxide (TiO_2) is demonstrated.

TiO_2 is a very attractive material because of its high refractive index and high transmission in visible range, yet requires very high pressure to make nanostructures via NIL. In this regard, a tactful method for TiO_2 patterning has been developed by introducing the solution-processable inorganic–organic hybrid TiO_2 precursor as an NIL resist [40, 41]. The organic parts in the resist can be thermally decomposed by annealing after NIL, leaving behind the patterned TiO_2 structure. Figure 8a shows the TiO_2 nanograting pattern fabricated as such. Controlling the annealing temperature additionally tunes the refractive indexes of TiO_2 (Fig. 8b); the thermal decomposition leads to increase the refractive index of the material. Also, the resulting TiO_2 nanograting pattern remains thinner compared with the original size made of a hybrid resist (Fig. 8c). The TiO_2 thin film and patterned area were free

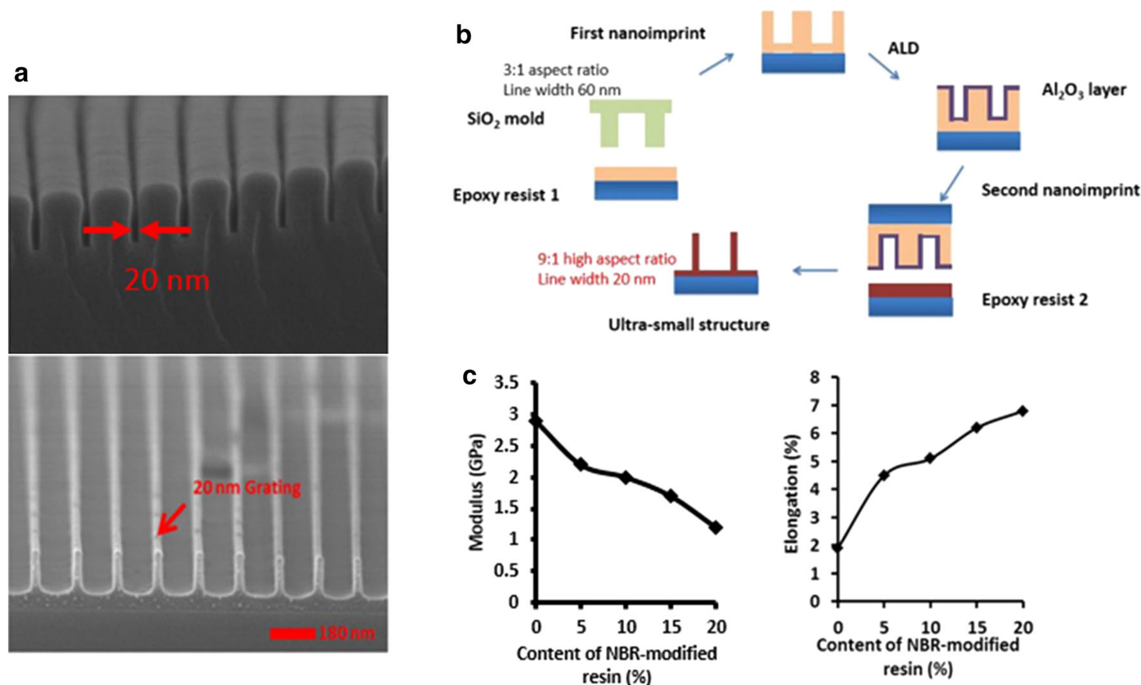

Fig. 7 **a** SEM image of *top*: trench nanomaster mold with atomic layer deposition (ALD) using alumina, *bottom*: ultra-small nanostructure. **b** Schematic draw of fabricating ultra-small nanostructure with ALD and two times nanoimprinting consecutively. **c** Properties of the cured epoxy resin containing different mixing ratios of bisphenol F-type epoxy resin and NBR-based epoxy resin which are modulus tunable (reproduced from Ref. [39] with permission from IOP Publishing)

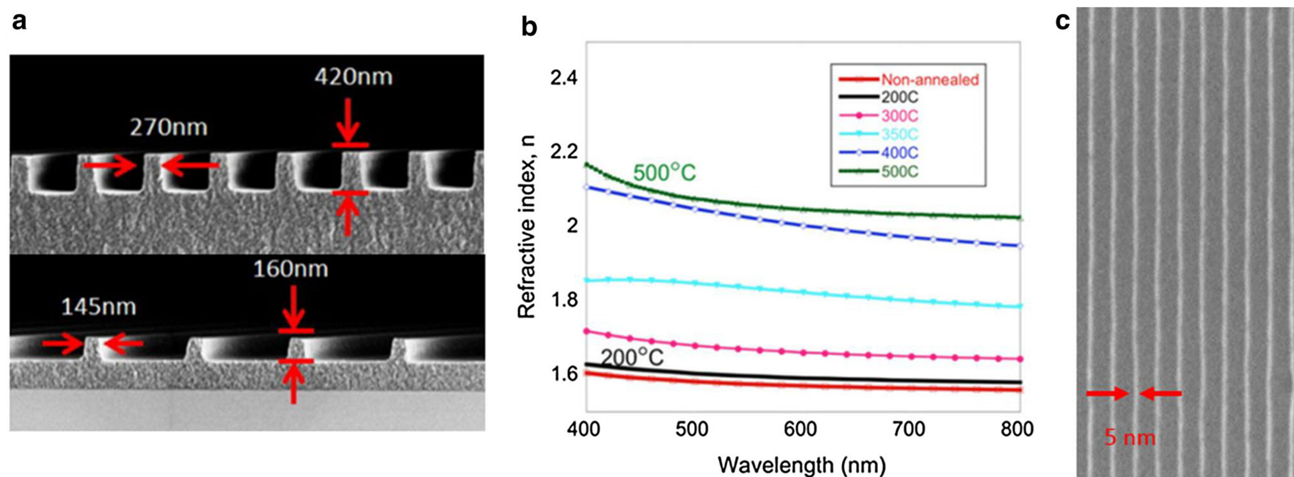

Fig. 8 **a** *Top*: cross section SEM of a 270 nm *line* width and 700 nm imprinted pitch gratings, *bottom*: SEM of the cross section after the annealing process at 400 °C for 10 min. The height of the pattern is decreased from 420 nm down to 160 nm after annealing. **b** Refractive index of TiO_2 films for various annealing temperatures. **c** SEM of the grating after annealing at 400 °C for 10 min. Original nanograting's width is 10 nm, and pitch is 40 nm (reproduced from Ref. [40] with permission from IOP Publishing)

from cracking after thermal annealing process while the thickness was less than 5 µm. Therefore, this approach can be versatile; the functional inorganic nanostructures of fine size resolution with tunable refractive index can be achieved, which could be applied for lots of applications ranging from nanoscale photonic devices to microscale lens and waveguides.

5 Application outlook

An array of applications requiring nanoscale patterns can be developed by capitalizing NIL and can move forward to commercially feasible levels by integrating the key technologies discussed above. Three of the most promising perspectives—photonics, electronics, and energy

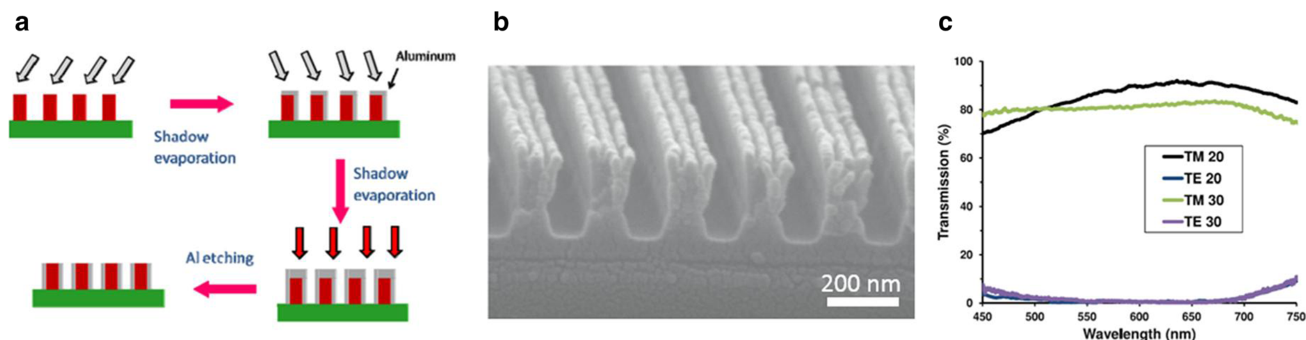

Fig. 9 **a** Schematic draw of fabricating wire-grid polarizer (WGP) with shadow evaporation. **b** SEM image of the WGP cross section. **c** TE and TM data of the WGP (reproduced from Ref. [67] with permission from IOP Publishing). The *numbers* in legend represents the deposited Al thicknesses

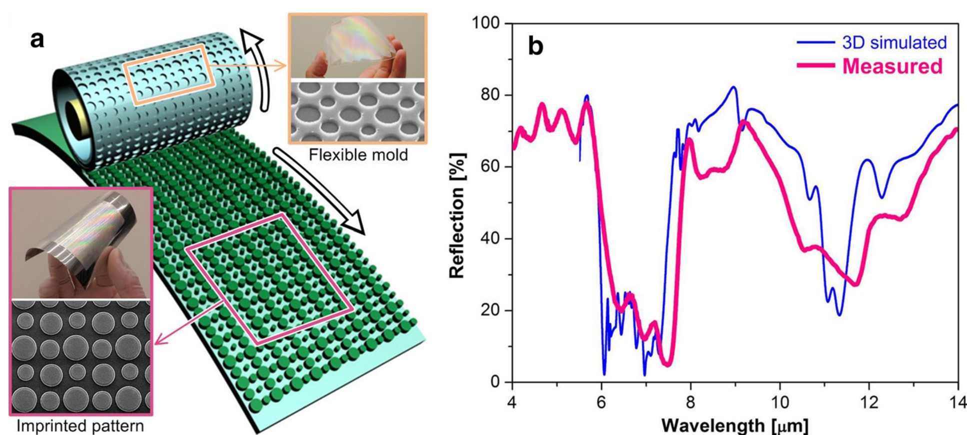

Fig. 10 **a** Schematics of the R2R NIL fabrication of a large-area plasmonic IR filter. A PDMS mold containing hole patterns continuously imprints the *dot patterns* on the MIM-stacked PET film. **b** Reflection spectra comparing simulation and measured results, indicating the broadband IR filtering performance (reproduced from Ref. [11] with permission from the American Institute of Physics)

systems—are categorized and presented below along with tangible and prospective applications.

5.1 Photonics

A polarizer, one of the most highly demanded photonic devices, can be fabricated in various formats and specifications by NIL. A metal wire-grid polarizer (WGP) simply comprising metal grating on a flexible substrate is one promising type of polarizers compared with popular polyvinyl alcohol (PVA)-based polarizers which should be made waterproof in thick protection frame (bezel) and suffer from heat loss; especially, for the flexible display development, the polarizer film component should be kept thin to ensure good bendability, for which WGPs can be a good alternative solution.

The working condition of WGPs in visible range requires the period of metal grating less than 200 nm, even down to 100 nm level for the best performance [42], making the slow and expensive e-beam lithography approach prohibitive. Instead, WGPs can be readily fabricated using NIL. It has been previously demonstrated that the bilayer metal WGP can be fabricated by evaporating an aluminum film over a NIL-patterned polymer grating [13]. Further improving the performance (e.g., transmission, extinction ratio), an angled metal evaporation can be adopted to cover the grating sidewalls only (i.e., shadow evaporation) [43], leaving the top part transparent. Figure 9 shows the WGP fabricated through the shadow evaporation over the NIL-patterned transparent grating, followed by the additional etching of top metal roofs, showing competitive performance.

Here, the double-evaporation enables the nanograting period as large as 220 nm, much larger than most of the commercialized WGPs, while the equivalent metal grating period is half as long after top etching; this is important in manufacturing viewpoint. The 220-nm-period grating can be imprinted much more easily and reliably than 110-nm-period pattering task. The WGP fabrication can be incorporated with R2R NIL for large-area application [8]. Additionally the fabricated WGPs can be encapsulated using such as PDMS to improve durability and biocompatibility [44, 45].

Various metamaterials and plasmonic devices can also be developed by the NIL fabrication of subwavelength-scale patterns [46]. Adopting R2R NIL, more scalable plasmonic metamaterial films can be continuously fabricated. For example, a large-area broadband IR filter can be devised using R2R NIL (Fig. 10) [11], where the subwavelength dot arrays are continuously patterned on the

metal–insulator–metal (MIM)-coated flexible polyethylene terephthalate (PET) substrate using a flexible PDMS mold (Fig. 10a). The patterned metal disks with varying diameters and submicron spacing on the insulator–metal layer indicate the desired broadband IR filtering characteristics (Fig. 10b).

5.2 Electronics

Semitransparent conductive materials, which have transparency in the visible range of electromagnetic spectrum, have been widely investigated for the electrode of optoelectronic devices such as photovoltaic (PV) cells and light-emitting diode (LED); especially, indium tin oxide (ITO) has been one of the most successful materials due to their superior conductivity and transparency. However, they are relatively brittle on the flexible substrate, inducing fractures on bent substrate, and high-conductivity ITO needs high-temperature annealing process, which is not suitable for plastic substrate; therefore, the necessity to the alternative approaches for flexible electronics has increased [47–49].

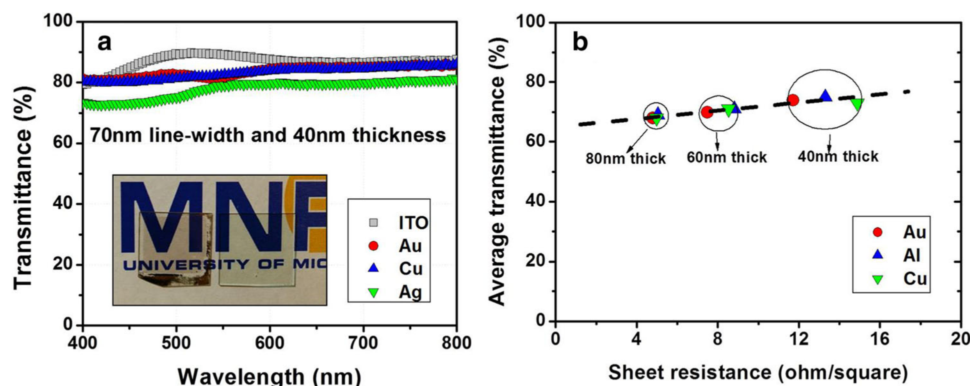

Fig. 11 **a** Optical transmittance of the ITO and transparent metal electrodes with a period of 700 nm and *line* width of 70 nm (reproduced from Ref. [51] with permission from John Wiley and Sons). **b** Average transmittance versus sheet resistance of transparent metal electrodes with a line width of 120 nm according to the thickness of metal (reproduced from Ref. [68] with permission from John Wiley and Sons)

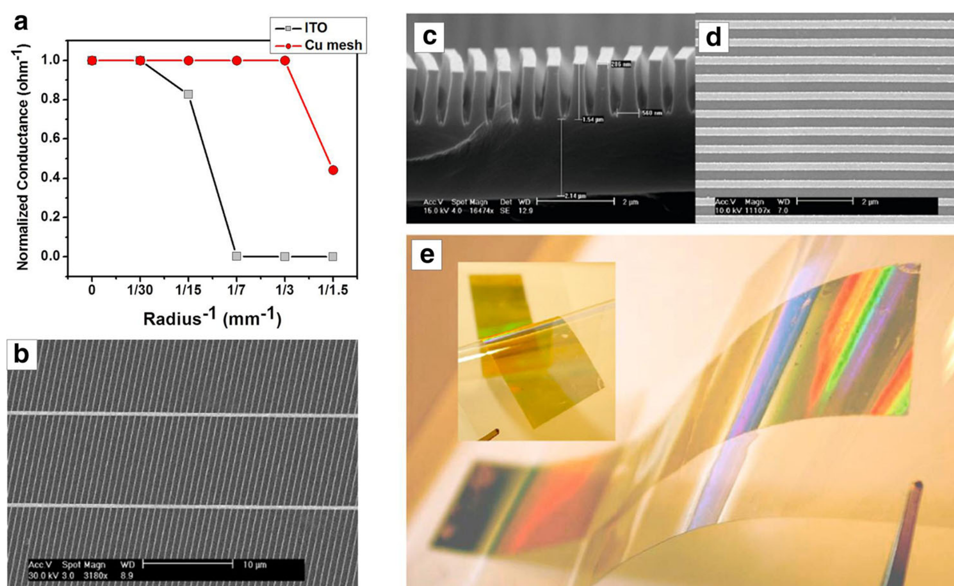

Fig. 12 **a** Normalized conductance versus inverse of the radius of curvature of the Cu wire mesh (*filled circle*) and the ITO electrode (*filled square*). The Cu mesh electrode on PEDOT:PSS-coated PET substrate showed a superior flexibility and can be bent to ~3 mm curvature with no degradation of conductance. **b** SEM images of Cu mesh electrode. (**c**–**e**) roll-to-roll transfer printing process: **c** SEM images of the imprinted epoxysilicon grating structure on the replicated flexible mold, **d** the transferred Au nanograting on UV-cured epoxy coated on a PET substrate, and **e** photograph of large-area (32 mm × 184 mm) Au nanogratings on UV-epoxy-coated PET substrate. *Inset* photograph shows the transparency of the Au nanogratings transferred to PET (reproduced from Ref. [52] with permission from Elsevier)

NIL-based metallic nanostructure can be a promising candidate to address the above-mentioned difficulties toward flexible large-area transparent conductor [50–53]. Firstly, transparent metal electrode (TME), composed of periodic metal wire grids, have high optical transparency as well as electrical conductivity. As shown in Fig. 11a, TMEs can have comparable transparency to the commercially available ITO electrode and the sheet resistance can be down to a few ohms per square level; especially, those properties can be adjusted by simply changing the width and thickness of metal lines in grid structures (Fig. 11b). Furthermore, TMEs show superior flexibility and durability. As shown in Fig. 12a, b, on the flexible substrate, Cu-based TME, which can be bent to about 3 mm radius of curvature without any conductance degradation, shows better flexibility than ITO, which shows the drastic decrease in conductance even about 30 mm radius [52]. To realize large-area transparent conductor, TME can be also extendable to roll-to-roll fabrication. Figure 12c–e show that Au metal nanograting structures on large-area PET substrate were successfully demonstrated using metal transfer technology-based roll-to-roll printing process [52]. We should mention that larger line width (~1 μm) metal grid is also useful, especially for robust large-area fabrication. In this regard, R2R NIL can be replaced by roller-based photo- and phase-shift lithography techniques that are suitable for large-area applications [54, 55].

5.3 Energy system

NIL-based periodic metal nanostructures, which exhibit unique optical properties such as the excitation of surface plasmon resonance (SPR), can be utilized to enhance the power conversion efficiency (PCE) of photovoltaic (PV) cells. Surface plasmons (SPs) are waves, of which electromagnetic field is confined to the vicinity of the metal/dielectric interface, and this confinement leads to an enhancement of the electromagnetic field at the interface when the condition of the resonance is fulfilled [56–58]. Therefore, those nanostructures can be potentially effective means to improve the efficiency of organic photovoltaics (OPVs) by enhancing the absorption of light even in a very

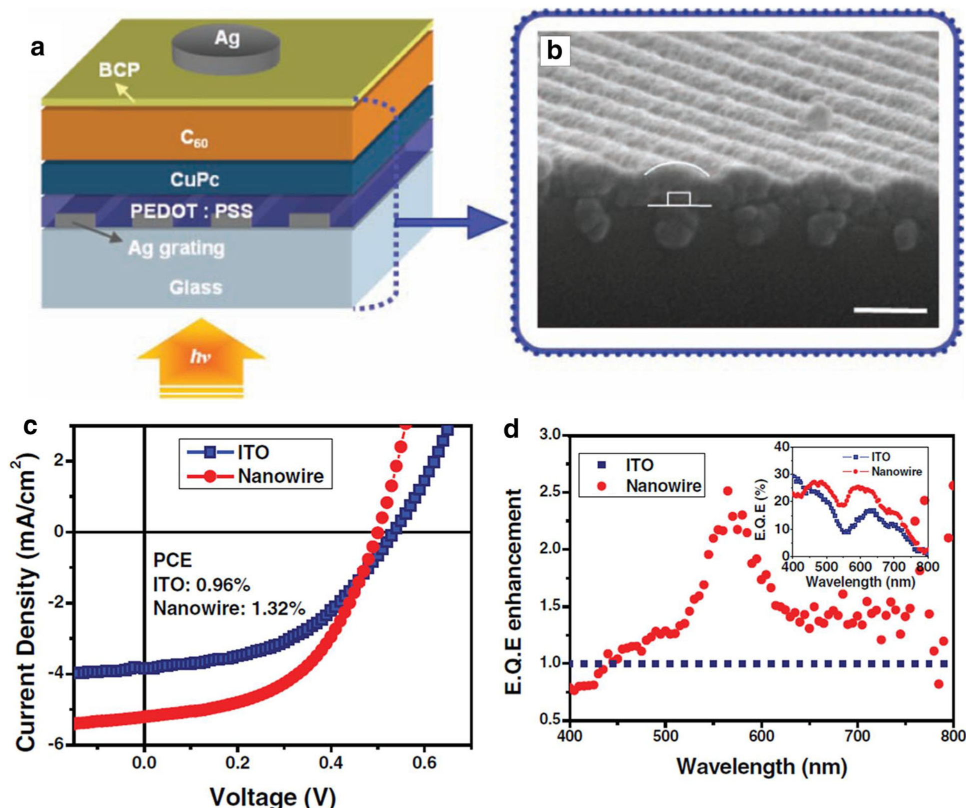

Fig. 13 **a** Schematic of the fabricated small molecular weight OPV cell. The fabricated devices have the layered structure of Ag nanowire anode, PEDOT:PSS, CuPc, C_{60}, BCP, and cathode (*thick* Ag film) from *bottom to top*. **b** Cross-sectional view of one of the fabricated devices, but without 70-nm-thick Ag cathode. Organic materials have the sinusoidal shape due to the height profile of the Ag nanowire array and the nature of thermal evaporation process. Organic layers are depicted with *solid lines,* and the *square* shows the position of the Ag nanowire on glass substrate. The *scale bar* is 200 nm. **c** *J-V* curve of the nanowire and control ITO devices. **d** External quantum efficiencies (EQE) enhancement of nanowire device with reference to ITO device. The inset gives the measured EQE of the nanowire and ITO devices (reproduced from Ref. [59] with permission from John Wiley and Sons)

thin organic semiconductor layer [50, 59]. This approach, in principle, can address the mismatch problems between the short exciton diffusion length in organic semiconductors (around 10 nm) and the large thickness required to fully absorb sunlight (e.g., hundreds of nanometers) [59–62]. Figure 13d shows the absorption enhancement from the NIL-based metal nanogratings, added to small molecule-based OPV cells (Fig. 13a, b), by SPR and waveguide effect, consequently leading to 40 % improved short circuit current (Fig. 13c) [59]. Those metal nanogratings work as

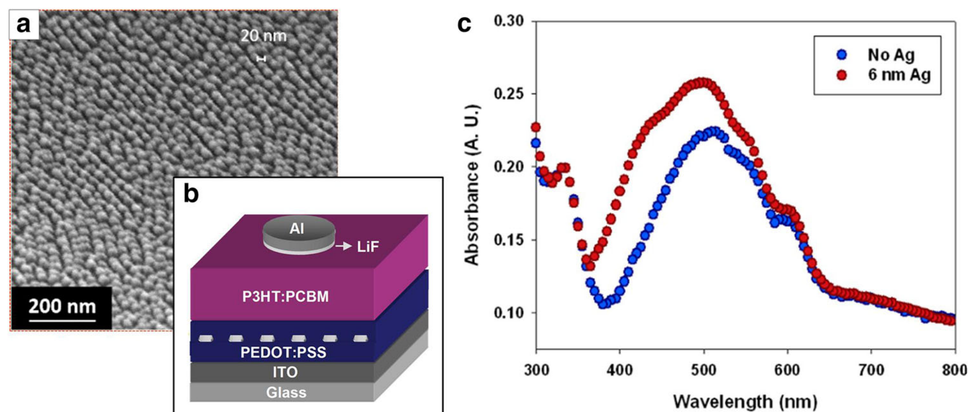

Fig. 14 **a** SEM of Ag plasmonic nanodot arrays deposited on nanodot-type PDMS stamp using angled deposition. **b** Schematic of the fabricated polymer PV cell. The fabricated PV cell has the configuration of ITO anode, Ag nanoparticle-embedded PEDOT:PSS, P3HT:PCBM blend and cathode (thick Al film with 1 nm LiF) from *bottom to top*. **c** Absorption spectra of photoactive layer with and without plasmonic Ag nanodot arrays (reproduced from Ref. [63] with permission from Elsevier)

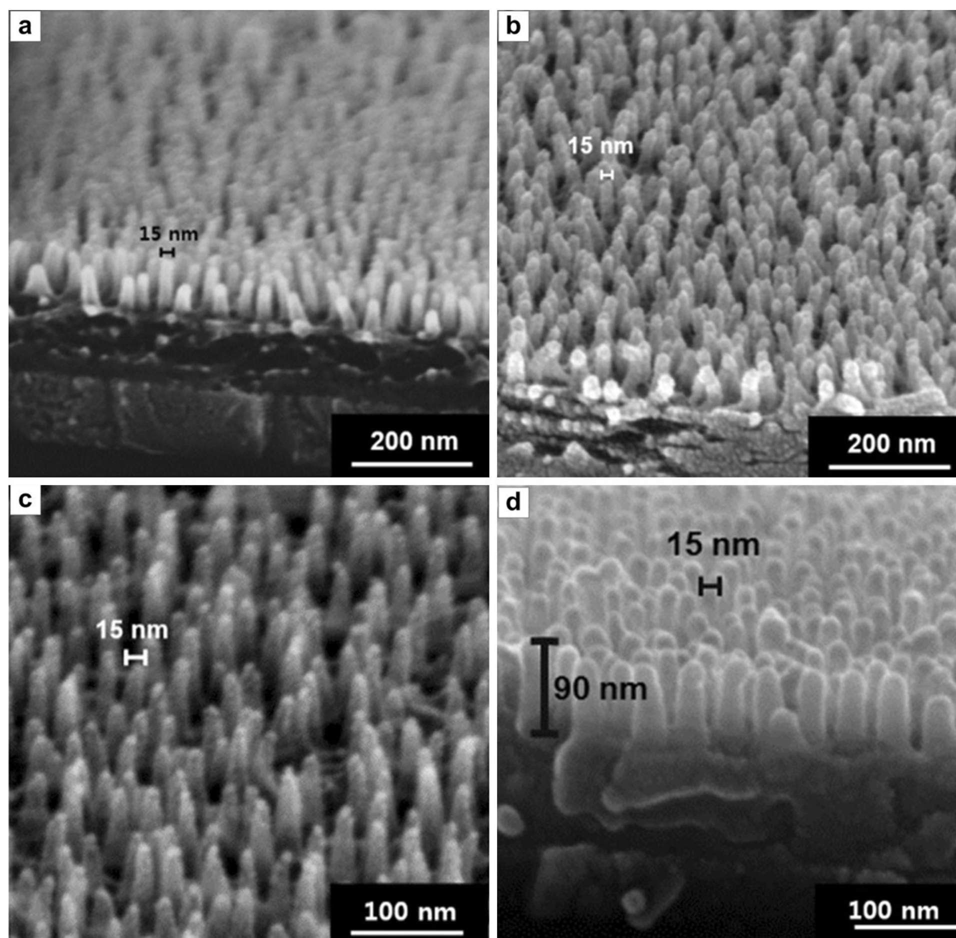

Fig. 15 High-aspect-ratio 15-nm-scale polymer semiconductor nanopillars: **a** poly[N-9″-hepta-decanyl-2,7-carbazole-alt-5,5-(4′,7′-di-2-thienyl-2′,1′,3′-benzothiadiazole)] (PCDTBT), **b** poly(indacenodithiophene-co-phenanthro[9,10-b]quinoxaline) (PIDT_PhanQ). High-aspect-ratio 15-nm-scale small molecular organic semiconductor nanopillars: **c** 2,4-bis[4-(N-phenyl-1-naphthylamino)-2,6-dihydroxyphenyl] squaraine (1-NPSQ), **d** fullerene derivative (reproduced from Ref. [64] with permission from John Wiley and Sons)

aforementioned TME as well as photonic nanostructures for absorption enhancement. Utilizing NIL process, nanoparticle-type plasmonic nanostructures can be also prepared. Figure 14 shows Ag plasmonic nanoparticles, fabricated by angled deposition on the nanoimprinted elastomeric stamps having dense 20-nm nanodot patterns. Those nanoparticles, expected to work as local field enhancer, could be added to OPV cells using metal transfer printing process and the resultant PV cells have about 10 % improved PCE [63].

NIL technology can be also utilized to introduce interdigitated electron donor and acceptor nanostructures into photoactive layer of OPV cells. By preparing nanostructures within tens of nanometer scale, comparable to exciton diffusion length of organic semiconductor, superior photoactive layer having efficient exciton dissociation and fast charge transport can be achieved. Figure 15 shows sub-20-nm-scale high-aspect-ratio organic semiconductor nanostructures, fabricated by solution-based soft-printing lithography [64]. Structural color filters utilizing the metallic nanostructures can be used to create more energy-efficient display platforms [65, 66]. This is another potential area of application for the R2R NIL-based technology.

6 Concluding remarks

We have discussed how NIL and R2R NIL may step toward more productive and widely applicable nanopatterning technology, particularly focusing on three key aspects. First, we have reviewed a series of scalable nanopatterning methods mainly derived from NIL based around the continuous traditional mechanical machining protocols. Then, we have investigated how the NIL molds of various shapes can be scaled up more practically and effectively, without complicated and costly aids. Lastly, developments of novel resist materials have been presented for more functional and smaller-period NIL patterning. As more methodologies specifically targeting large-area and high-throughput nanopatterning emerge along with these foundational NIL technology components, nanopattern fabrication will enter the manufacturing level that could lead to a myriad of useful applications in electronics, sensing, photonics, and energy conversion.

Acknowledgments This work was supported by the NSF grant CMMI 1025020 through the subcontract from University of Massachusetts, Amherst. JGO acknowledges the support by the Research Program funded by the Seoul National University of Science and Technology. HJP acknowledges the support by Nano Material Technology Development Program through the National Research Foundation of Korea (NRF) funded by the Ministry of Science, ICT and Future Planning. (2009-0082580), and the support by the Basic Science Research Program through the National Research Foundation of Korea (NRF) funded by the Ministry of Education (2014R1A1A2056403). YJS acknowledges the support by Multidisciplinary University Research Initiatives (MURI) Program and Korean Pioneer Project funded by the National Research Foundation of Korea (NRF).

References

1. L.J. Guo, Adv. Mater. **19**(4), 495 (2007)
2. H. Schift, J. Vac. Sci. Technol. B **26**(2), 458 (2008)
3. S.Y. Chou, P.R. Krauss, P.J. Renstrom, Science **272**(5258), 85 (1996)
4. H.C. Scheer, N. Bogdanski, M. Wissen, S. Mollenbeck, Microelectron. Eng. **85**(5–6), 890 (2008)
5. M. Bender, A. Fuchs, U. Plachetka, H. Kurz, Microelectron. Eng. **83**(4–9), 827 (2006)
6. H.B. Lan, H.Z. Liu, J. Nanosci. Nanotechnol. **13**(5), 3145 (2013)
7. J.J. Dumond, H.Y. Low, J. Vac. Sci. Technol. B **30**(1), 010801 (2012)
8. J.G. Ok, S.H. Ahn, M.K. Kwak, L.J. Guo, J. Mater. Chem. C **1**(46), 7681 (2013)
9. S.H. Ahn, L.J. Guo, Adv. Mater. **20**(11), 2044 (2008)
10. S.H. Ahn, L.J. Guo, ACS Nano **3**(8), 2304 (2009)
11. J.G. Ok, H.S. Youn, M.K. Kwak, K.T. Lee, Y.J. Shin, L.J. Guo, A. Greenwald, Y.S. Liu, Appl. Phys. Lett. **101**(22), 4 (2012)
12. H.J. Park, M.G. Kang, S.H. Ahn, L.J. Guo, Adv. Mater. **22**(35), E247 (2010)
13. S.H. Ahn, J.S. Kim, L.J. Guo, J. Vac. Sci. Technol. B **25**(6), 2388 (2007)
14. S.H. Ahn, L.J. Guo, Nano Lett. **9**(12), 4392 (2009)
15. J.G. Ok, H.J. Park, M.K. Kwak, C.A. Pina-Hernandez, S.H. Ahn, L.J. Guo, Adv. Mater. **23**(38), 4444 (2011)
16. S.H. Ahn, J.G. Ok, M.K. Kwak, K.T. Lee, J.Y. Lee, L.J. Guo, Adv. Funct. Mater. **23**(37), 4739 (2013)
17. J.G. Ok, A. Panday, T. Lee, L.J. Guo, Nanoscale **6**(24), 14636 (2014)
18. C. Ross, Annu. Rev. Mater. Res. **31**, 203 (2001)
19. C.C. Striemer, T.R. Gaborski, J.L. McGrath, P.M. Fauchet, Nature **445**(7129), 749 (2007)
20. H.J. Park, M.G. Kang, L.J. Guo, ACS Nano **3**(9), 2601 (2009)
21. M.K. Kwak, J.G. Ok, S.H. Lee, L.J. Guo, Mater. Horiz. **2**(1), 86 (2015)
22. S.J. Choi, H.N. Kim, W.G. Bae, K.Y. Suh, J. Mater. Chem. **21**(38), 14325 (2011)
23. C.R. Martin, Science **266**(5193), 1961 (1994)
24. T. Shimizu, T. Xie, J. Nishikawa, S. Shingubara, S. Senz, U. Gosele, Adv. Mater. **19**(7), 917 (2007)
25. C.J. Hawker, T.P. Russell, MRS Bull. **30**(12), 952 (2005)
26. F.S. Bates, G.H. Fredrickson, Annu. Rev. Phys. Chem. **41**, 525 (1990)
27. E. Huang, L. Rockford, T.P. Russell, C.J. Hawker, Nature **395**(6704), 757 (1998)
28. D.Y. Ryu, K. Shin, E. Drockenmuller, C.J. Hawker, T.P. Russell, Science **308**(5719), 236 (2005)
29. J.N.L. Albert, T.H. Epps, Mater. Today **13**(6), 24 (2010)
30. S.W. Hong, X.D. Gu, J. Huh, S.G. Xiao, T.P. Russell, ACS Nano **5**(4), 2855 (2011)
31. K.J. Morton, G. Nieberg, S. Bai, S.Y. Chou, Nanotechnology **19**(34), 345301 (2008)
32. C. Pina-Hernandez, L.J. Guo, P.-F. Fu, ACS Nano **4**(8), 4776 (2010)
33. C. Pina-Hernandez, P.-F. Fu, L.J. Guo, ACS Nano **5**(2), 923 (2011)

34. T. Asefa, M.J. MacLachlan, H. Grondey, N. Coombs, G.A. Ozin, Angew. Chem. **112**(10), 1878 (2000)
35. D. Morecroft, J.K. Yang, S. Schuster, K.K. Berggren, Q. Xia, W. Wu, R.S. Williams, J. Vac. Sci. Technol. B **27**(6), 2837 (2009)
36. S.Y. Chou, P.R. Krauss, W. Zhang, L. Guo, L. Zhuang, J. Vac. Sci. Technol. B **15**(6), 2897 (1997)
37. E. Delamarche, H. Schmid, B. Michel, H. Biebuyck, Adv. Mater. **9**(9), 741 (1997)
38. B.K. Lee, N.G. Cha, L.Y. Hong, D.P. Kim, H. Tanaka, H.Y. Lee, T. Kawai, Langmuir **26**(18), 14915 (2010)
39. Y.J. Shin, Y.-K. Wu, L.J. Guo, Nanotechnology **24**(25), 255302 (2013)
40. C. Pina-Hernandez, V. Lacatena, G. Calafiore, S. Dhuey, K. Kravtsov, A. Goltsov, D. Olynick, V. Yankov, S. Cabrini, C. Peroz, Nanotechnology **24**(6), 065301 (2013)
41. R. Ganesan, J. Dumond, M.S. Saifullah, S.H. Lim, H. Hussain, H.Y. Low, ACS Nano **6**(2), 1494 (2012)
42. S.-W. Ahn, K.-D. Lee, J.-S. Kim, S.H. Kim, J.-D. Park, S.-H. Lee, P.-W. Yoon, Nanotechnology **16**(9), 1874 (2005)
43. Y.J. Shin, C. Pina-Hernandez, Y.-K. Wu, J.G. Ok, L.J. Guo, Nanotechnology **23**(34), 344018 (2012)
44. Y.J. Shin, Y.K. Wu, K.T. Lee, J.G. Ok, L.J. Guo, Adv. Opt. Mater. **1**(11), 863 (2013)
45. A.E. Hollowell, L.J. Guo, Adv. Opt. Mater. **1**(4), 343 (2013)
46. A. Boltasseva, J. Opt. Pure Appl. Opt. **11**(11), 114001 (2009)
47. B. Maennig, J. Drechsel, D. Gebeyehu, P. Simon, F. Kozlowski, A. Werner, F. Li, S. Grundmann, S. Sonntag, M. Koch, K. Leo, M. Pfeiffer, H. Hoppe, D. Meissner, N.S. Sariciftci, I. Riedel, V. Dyakonov, J. Parisi, Appl Phys Mater. Sci Process. **79**(1), 1 (2004)
48. Z. Chen, B. Cotterell, W. Wang, E. Guenther, S.J. Chua, Thin Solid Films **394**(1–2), 202 (2001)
49. M.W. Rowell, M.A. Topinka, M.D. McGehee, H.J. Prall, G. Dennler, N.S. Sariciftci, L.B. Hu, G. Gruner, Appl. Phys. Lett. **88**(23), 233506 (2006)
50. M.G. Kang, H.J. Park, S.H. Ahn, T. Xu, L.J. Guo, IEEE J. Sel. Top. Quantum Electron. **16**(6), 1807 (2010)
51. M.G. Kang, M.S. Kim, J.S. Kim, L.J. Guo, Adv. Mater. **20**(23), 4408 (2008)
52. M.G. Kang, H.J. Park, S.H. Ahn, L.J. Guo, Sol. Energy Mater. Sol. Cells **94**(6), 1179 (2010)
53. H.J. Park, T. Xu, J.Y. Lee, A. Ledbetter, L.J. Guo, ACS Nano **5**(9), 7055 (2011)
54. J.G. Ok, M.K. Kwak, C.M. Huard, H.S. Youn, L.J. Guo, Adv. Mater. **25**(45), 6554 (2013)
55. M.K. Kwak, J.G. Ok, J.Y. Lee, L.J. Guo, Nanotechnology **23**(34), 6 (2012)
56. H.A. Atwater, A. Polman, Nat. Mater. **9**(3), 205 (2010)
57. E. Ozbay, Science **311**(5758), 189 (2006)
58. W.L. Barnes, A. Dereux, T.W. Ebbesen, Nature **424**(6950), 824 (2003)
59. M.G. Kang, T. Xu, H.J. Park, X.G. Luo, L.J. Guo, Adv. Mater. **22**(39), 4378 (2010)
60. H.J. Park, H. Kim, J.Y. Lee, T. Lee, L.J. Guo, Energy Environ. Sci. **6**(7), 2203 (2013)
61. H.J. Park, J.Y. Lee, T. Lee, L.J. Guo, Adv. Energy Mater. **3**(9), 1135 (2013)
62. W.A. Luhman, R.J. Holmes, Adv. Funct. Mater. **21**(4), 764 (2011)
63. H.J. Park, L.J. Guo, Chin. Chem. Lett. **26**, 419 (2015)
64. H. Youn, H.J. Park, L.J. Guo, Energy Technol. **3**, 340 (2015)
65. T. Xu, Y.K. Wu, X.G. Luo, L.J. Guo, Nat. Commun. **1**, 59 (2010)
66. Y.K.R. Wu, A.E. Hollowell, C. Zhang, L.J. Guo, Sci. Rep. **3**, 1194 (2013)
67. Y.J. Shin, C. Pina-Hernandez, Y.K. Wu, J.G. Ok, L.J. Guo, Nanotechnology **23**(34), 6 (2012)
68. M.G. Kang, L.J. Guo, Adv. Mater. **19**(10), 1391 (2007)